

**Classification: Biological Sciences / Biophysics**

# **Domain Compliance and Elastic Power Transmission in Rotary F<sub>0</sub>F<sub>1</sub>-ATPase**

**Hendrik Sielaff<sup>1</sup>, Henning Rennekamp<sup>1</sup>, André Wächter<sup>1,2</sup>, Hao Xie<sup>1</sup>, Florian Hilbers<sup>1</sup>,  
Katrin Feldbauer<sup>1,3</sup>, Stanley D. Dunn<sup>4</sup>, Siegfried Engelbrecht<sup>1,2</sup> and Wolfgang Junge<sup>1\*</sup>**

<sup>1</sup> *Department of Biophysics, University of Osnabrück, 49069 Osnabrück, Germany*

<sup>2</sup> *Department of Biochemistry, University of Osnabrück, 49069 Osnabrück, Germany*

<sup>3</sup> *present address: Max-Planck-Institute of Biophysics, 60438 Frankfurt, Germany*

<sup>4</sup> *Dept. Biochemistry, University of Western Ontario, London, Ontario N6A 5C1, Canada*

**\* corresponding author**

Tel +49-541-969-2872

Fax -12872

Email [junge@uos.de](mailto:junge@uos.de)

Courier Universität Osnabrück, FB Biologie/Chemie, R.35/42,  
Barbarastr. 11, D-49076 Osnabrück, Germany

## Abstract

The two nanomotors of rotary ATP synthase, ionmotive  $F_O$  and chemically active  $F_1$ , are mechanically coupled by a central rotor and an eccentric bearing. Both motors rotate, with 3 steps in  $F_1$  and 10-15 in  $F_O$ . Simulation by statistical mechanics has revealed that an elastic power transmission is required for a high rate of coupled turnover. Here we investigated the distribution in the  $F_O F_1$ -structure of compliant and stiff domains. The compliance of certain domains was restricted by engineered disulfide bridges between rotor and stator, and the torsional stiffness ( $\kappa$ ) of unrestricted domains was determined by analyzing their thermal rotary fluctuations. A fluorescent magnetic bead was attached to single molecules of  $F_1$ , and a fluorescent actin filament to  $F_O F_1$ , respectively. They served to probe first the functional rotation, and, after formation of the given disulfide bridge, the stochastic rotational motion. Most parts of the enzyme, in particular the central shaft in  $F_1$ , and the long eccentric bearing were rather stiff (torsional stiffness  $\kappa > 750$  pNm). One domain of the rotor, namely where the globular portions of subunits  $\gamma$  and  $\epsilon$  of  $F_1$  contact the c-ring of  $F_O$ , was more compliant ( $\kappa \cong 68$  pNm). This elastic buffer smoothes the co-operation of the two stepping motors. It is located where needed, between the two sites where the power-strokes in  $F_O$  and  $F_1$  are generated and consumed.

\body

## Introduction

Molecular motors abound in the cell. It is worth asking whether or not a discrete power stroke, usually caused by the hydrolysis of ATP or the transport of an ion, is fine tuned to the detailed molecular events which are powered by the respective motor. In ATP synthase ( $F_0F_1$ -ATPase), for instance, the rotary electromotor,  $F_0$ , drives the rotary chemical generator,  $F_1$ , to synthesize ATP. Whereas  $F_0$ , depending on the organism, processes in 11-15 steps per turn,  $F_1$  processes in 3 steps. As an alternative to the fine tuning of the underlying partial reactions it has been proposed for long ((1-4) and references therein) that an elastic power transmission might serve to smooth the coupled operation of the counteracting rotary motors. To substantiate this claim here we determined the distribution of stiff and compliant domains over the molecular structure of this enzyme.

The ATP synthase from *Escherichia coli*,  $EF_0F_1$ , is composed from eight different subunits attributable either to the 'rotor', namely subunits  $\gamma$  and  $\epsilon$  of  $F_1$  plus the  $c_{10}$ -ring of  $F_0$  (5), or to the 'stator', namely subunits  $\delta$  and  $(\alpha\beta)_3$  of  $F_1$ , plus subunits  $a$  and  $b_2$  of  $F_0$ . The rotor portion of  $F_1$  is linked to the rotor portion of the ion-motive  $F_0$  by interfacing subunits  $\gamma$  and  $\epsilon$  of  $F_1$  with the  $c$ -ring of  $F_0$ . The crystal structure of the bovine mitochondrial  $F_1$  ( $MF_1$ ) (6) has revealed the threefold pseudo-symmetry of the hexagon formed by subunits  $\alpha$  and  $\beta$ , which are arranged as  $(\alpha\beta)_3$ . Under ATP hydrolysis the structural symmetry of three is paralleled by the rotation of the  $\gamma$  subunit in three steps of  $120^\circ$  with substeps of  $40^\circ$  and  $80^\circ$  (7-9). The  $c$ -ring ion-driven motor,  $F_0$ , contains 10-15 identical monomers depending on the organism and supposedly steps by  $24^\circ$  -  $36^\circ$ . The symmetry does match in some organisms (3:15) but not in others (e.g. 3:14 in chloroplast  $CF_0F_1$  and 3:10 in yeast and *E. coli*) (see (10-12) and references therein).

First evidence for an elastic coupling element in  $F_0F_1$  has been provided by simulations of its kinetic properties both under rate limitation by proton transfer in  $F_0$  (13) and by catalysis in  $F_1$

(14). A first estimate for the torsional stiffness of the elastic element in  $EF_0F_1$  has been obtained from recordings of the torque as a function of the angular reaction coordinate (4). A single molecule of  $F_0F_1$  has been immobilized with  $F_1$  down on a solid support with a fluorescent actin filament attached to the c-ring of  $F_0$  to monitor the rotation as driven by the hydrolysis of ATP. Because of the viscous drag on the long filament (length  $>3 \mu\text{m}$ ) the turnover rate is reduced by more than two orders of magnitude compared to the rate without filament. The viscous drag counteracts the enzyme generated torque and this bends the filament. Like with a spring balance its curvature was used to determine the torque as a function of the angular position of the c-ring. Although the driving motor,  $F_1$ , progressed in steps (of  $120^\circ$ ), the torque profile, as sensed by  $F_0$ , was smooth, and this was attributed to an elastic coupling element with a torsional stiffness of about 60 pNnm (4). The theoretical treatment of this nanomachine in terms of the Smoluchowski equation of statistical mechanics has revealed the benefit of an elastic buffer, which is required for a high turnover rate under load (see Fig. 8 in (4), and also (15)). Although the existence of an elastic power transmission between  $F_0$  and  $F_1$  has been established by the above cited work (4) the magnitude and the distribution of compliant *versus* stiff elements over the enzyme structure, in particular between central rotor and eccentric stator, has not been determined before. Here, we investigated the torsional stiffness of several enzyme domains by fluctuation analysis, and localized the elastic buffer in the structure of  $EF_0F_1$ . The domain compliance was investigated by monitoring either via a magnetic bead (diameter typ.  $1 \mu\text{m}$ ) or by a short actin filament (length  $<0.5 \mu\text{m}$ ) the thermal rotational fluctuations of an attached fluorescent probe in immobilized single molecules. In order to attribute the observed overall compliance to specific enzyme domains we stiffened selected portions by disulfide cross-linking through engineered cysteines. The properties of the respective cysteine pairs, their position in the crystal structure and the correlation between the functional halt positions of the active enzyme, the disulfide-locked conformations, and the published crystal structures have been presented elsewhere (46).

## RESULTS

**Magnetically driven rotation and rotational fluctuations in EF<sub>1</sub>** were studied as follows. A single molecule of EF<sub>1</sub> was immobilized on a Ni-NTA-coated glass plate by an engineered His-tag at the N-terminal end of each of the three copies of subunit  $\beta$  as illustrated in Fig.1A. A streptavidin-coated hyper-paramagnetic bead was attached with a biotin-maleimide function to the rotor via an engineered cysteine in the bulky protruding domain of subunit  $\gamma$  ( $\gamma$ K109C). The bead, typical diameter 1  $\mu$ m, was fluorescence-labeled by biotinylated quantum-dots (Q-dots), allowing for extended observation times without bleaching. A slowly rotating magnetic field (typ. 0.1 rev/s) was applied (5 mM Mg-ATP present), and the orientation of the bead was videographed in an inverted fluorescence microscope. If the viewing field contained, say 100 beads total, it typically showed 95 rotating ones. Whether or not this was a relevant, enzyme-related rotation was checked as follows. Aside from the above mentioned cysteine serving to attach the bead, the mutant-EF<sub>1</sub> contained two further cysteines, they were engineered to form a zero-length cross link between rotor and stator under oxidizing conditions. Placed opposite to each other in the homology structure of EF<sub>1</sub> to the crystal structure of MF<sub>1</sub> (6). The location of these cysteines in the enzyme structure is indicated in Fig. 1. The magnetically driven rotation of the beads stopped after perfusion of the reaction chamber with an oxidant while the rotating field was still on. Fig. 1B shows the percentage of rotating over total beads in the viewing field as function of three cycles where the solution over the glass plate was changed from reducing to oxidizing and back. The loss of rotating beads from one redox-cycle to the other was due to the detachment of beads/enzymes from the solid support by the shear flow during exchange of solution. It was obvious from Fig. 1B that (i) the formation and cleavage of the disulfide bonds was reversible, and (ii) that the rotation of the great majority of beads was related to the rotation of subunit  $\gamma$  in the  $(\alpha\beta)_3$ -corpus of EF<sub>1</sub>. In other words the data excluded that the bead/EF<sub>1</sub>-construct rotated as a whole (around one His-tag), that beads were dancing around their

attachment sites on EF<sub>1</sub>, or, unattached to F<sub>1</sub>, around an unspecific attachment site on the glass surface.

Keeping one particular rotating bead in focus its enzyme molecule was locked by changing the solution from reducing to oxidizing. Then the magnetic field was switched off. As a consequence, the bead only showed rotary thermal fluctuations of rather narrow width. The probability distribution of these fluctuations was determined and fitted by a single Gaussian. Two such histograms are shown in Fig. 1C. The distribution was wider for the double mutant  $\alpha$ E284C/ $\gamma$ A270C (in magenta) than for the double mutant  $\beta$ D380C/ $\gamma$ A87C (in green). Good reproducibility of this width from one single molecule of a given mutant enzyme to the other (see Fig. S1 in the supplement) showed that the different widths between these two mutants was meaningful.

One might ask whether the rotational fluctuation of the large bead, its diameter being by two orders of magnitude greater than the one of the enzyme, are restricted by the enzyme's compliance or rather by surface contacts. Three lines of evidence showed that the fluctuations of the bead was related to the enzyme and thus relevant. (i) The width of the thermal fluctuations was reproducibly (see Fig. S1) related to the position in the enzyme of the respective disulfide bridge (see Fig. 1C). (ii) Only occasionally, we observed beads that were stuck at the surface and this was immediately evident from a much narrower width of their fluctuations, typical full width at half maximum (FWHM)  $<3^\circ$ , as compared with  $>7^\circ$  in the great majority of cases (see Fig. S2 in the supplement). (iii) In our related study on the orientation of the rotor during functional halts in comparison with its orientation as revealed by X-ray crystallography of the inhibited enzyme (46) we found that the difference between the 'enzyme-intrinsic' stop-orientations, e.g. after ADP-saturation, and after oxidation of an engineered cysteine pair (engineered stop) were strictly dependent on the position of the particular cysteine on the helical wheel of subunit  $\gamma$  (see Fig. S3 in the supplement). It excluded that these stop positions were dominated by surface contacts.

**Rotary fluctuations and the torsional stiffness.** When a homogeneous, isotropic elastic rod is fixed at one end, while being free at the other end, the thermal impact on the rod (the Langevin force) generates a fluctuating torque,  $M$ . It torsionally strains the free surface by an angle  $\phi$  (in radian), such that  $M = \kappa \cdot \phi$ . The torsional stiffness of the rod,  $\kappa$ , comes in units of pNnm. The elastic energy which is transiently stored in the rod is  $U = 1/2 \cdot \kappa \cdot \phi^2$ , and the probability,  $p(\phi)$ , to find a given deformation angle is given by Boltzmann's equation

$$(1) \quad p(\phi) = \text{const} \cdot \exp\left(-\frac{U}{k_B T}\right) = (2\pi \cdot \sigma^2)^{-1/2} \cdot \exp\left(-\frac{\phi^2}{2\sigma^2}\right)$$

yielding a Gaussian whose variance,  $\sigma^2$ , reads:

$$(2) \quad \sigma^2 = k_B T \cdot \kappa^{-1}$$

If the elastic element is composed from two rods of different stiffnesses,  $\kappa_1$  and  $\kappa_2$ , the resulting variance is the sum of the two reciprocal stiffnesses, again calibrated in terms of  $k_B T$ .

$$(3) \quad \sigma_{\text{comp}}^2 = k_B T \cdot (\kappa_1^{-1} + \kappa_2^{-1}) = k_B T \cdot \kappa_{\text{result}}^{-1}$$

If, instead of the standard deviation,  $\sigma$ , in radian, the FWHM of the distribution in degrees is read out, the stiffness,  $\kappa$ , reads as follows:

$$(4) \quad \kappa = 8 \cdot \ln 2 \cdot \left(\frac{180}{\pi}\right)^2 \cdot k_B T \cdot (FWHM)^{-2} \cong 73700 \text{ pNnm} \cdot (FWHM)^{-2}$$

In summary: (i) The width of rotational fluctuations yields the torsional stiffness calibrated in terms of  $k_B T$ . (ii) In composite rods the reciprocal stiffnesses are additive. (iii) The most compliant element stores the major portion of the elastic deformation energy, and it contributes most to the deformation angle.

**The torsional compliance of the rotor-portion in EF<sub>1</sub>.** The evaluation of the original data shown in Fig. 1C according to Eq. (2) yielded a stiffness of about 1500 pNnm for the mutant  $\beta\text{D380C}/\gamma\text{A87C}$ , where the disulfide link was placed close to the bead (green), and 500 pNnm for the mutant  $\alpha\text{E284C}/\gamma\text{A270C}$  (magenta), where it was farther down. The greater figure in the former mutant comprised compliance from all elements of the surface-to-enzyme-to-bead

construct, in particular the rotational compliance of the His-tags, and of the bead's attachment to the central shaft. All these "background compliances" were small, the enzyme body and its attachment to the surface were stiff. The great stiffness was partially relieved in the mutant where the rotor/stator lock was placed farther down towards the C-terminal end of subunit  $\gamma$  (Fig. 1C, magenta). The increase of the compliance was thus attributable to the portion of subunit  $\gamma$  lying between the two sites chosen for blocking the rotation. We calculated a stiffness of  $\kappa = 750$  pNnm for the particular portion of the central stalk lying between the "green" and "magenta" encircled sites as shown in Fig. 1C.

**The torsional compliance of the rotor-portion in the holoenzyme,  $EF_0F_1$ ,** was determined by a similar procedure as for  $EF_1$  except for two modifications, (i) ATP-driven (0.05-5 mM Mg-ATP) instead of magnetically-driven rotation served to select relevant single molecules, and (ii) a fluorescent actin filament attached to the c-ring of  $F_0$  served as a probe. This construct is illustrated in Fig. 2A. Detergent-solubilized  $EF_0F_1$  was immobilized by His-tags. A fluorescent actin filament was attached to  $EF_0$ -c<sub>10</sub> by biotin/streptactin linkage to engineered Strep-tags at the C-termini of  $EF_0$ -c (16). The rotation of the c<sub>10</sub>-ring, driven by ATP hydrolysis, was recorded by micro-videography. Short filaments (typ. 0.5  $\mu$ m) were used to avoid viscous over-damping of the stepped rotation (17) (4). Oxidizing conditions promoted the formation of a disulfide bridge between appropriately engineered cysteines on the stator and the rotor (see Fig. 2B), and this blocked the rotation.

Keeping a given rotating enzyme molecule in focus and changing the solution from reducing to oxidizing stopped the rotation. The rotational fluctuations persisted and were attributable to fluctuations within the enzyme. The short actin filament itself contributed negligibly (see (17) for the length dependence of fluctuations).

The inset in Fig. 2B shows the location of the disulfide bridge in three mutants, namely (i)  $\alpha$ 1223CcL72C (blue), (ii)  $\beta$ D380C  $\gamma$ A87C (green), and (iii)  $\alpha$ E284C $\gamma$ A276C (red). The probability distributions of the respective rotational fluctuations are shown in matching colors in



Fig. 2B. The respective FWHM translated into the following figures for the torsional stiffness in pNnm: (i) 450 (blue), (ii) 59 (green), and (iii) 47 (red). It implied a stiffness of <68 pNnm for the rotor segment lying between the blue and the green disulfide bridge. The stiffness of the segment between the green and the red disulfide bridge was here not to be determined precisely because of the great compliance of the segment farther up towards  $F_0$ .

The largest stiffness resulted if the **c**-ring was locked to subunit **a** (blue in Fig. 2B). The stiffening effect of this particular cross link showed that the respective detergent-solubilized and surface-attached  $EF_0F_1$  construct was intact, in particular that the attachment of the stator to the rotor was present. This qualifies the previous notion of a dangling stator in this  $EF_0F_1$ -construct (18). The smaller stiffness (450 pNnm) compared with the one observed with magnetic beads for  $F_1$  (1500 pNnm) was attributable to the compliance of the **c**-ring/ $F$ -actin construct. It was not owed to the attachment of  $F_1$  to the solid support (see data in Fig. 1C).

**The torsional compliance of the unrestricted, active enzyme**, e.g. during one ATP-waiting dwell before jumping by  $120^\circ$  into the next dwell was inferred from long trajectories of rotation. Fig. 3A shows a short segment of a stepped rotary trajectory of 2 s duration, and Fig. 3B the respective angular probability distribution. The stiffness of the ADP-saturated and thereby intrinsically locked state (orange in Fig. 3B) was 66 pNnm, very much the same as when the DELSEED lever was cross linked with the rotor (68 pNnm, green data in Fig. 2B). During the ATP-waiting dwells (typically of 100 ms duration, blue in Fig. 3B) the stiffness was  $\kappa = 30$  pNnm. It implied that the lever motion (occurring during the ATP-wait) contributed a stiffness of 50 pNnm.

**The torsional compliance of the eccentric bearing** was investigated in a construct which is illustrated in Fig. 4A. A cysteine was added to the C-terminal end of subunit **b** (bold letters in **NCMNLN**.....). Two cysteines, one on each copy of the more or less parallel helices of subunit **b** (19-21), served as attachment sites for a Q-dot doped magnetic bead via the maleimide-biotin link. Fig. 4B shows the probability distribution of the bead without magnetic field (top) and with the magnetic field turning steadily at 0.125 rev/s either clockwise (blue) or counter-clockwise

(red) when viewed from the  $F_O$ -side. The sign of the displacement was chosen positive when moving in the counter-clockwise direction. As expected, the rotational freedom of the bead in response to the magnetic field was limited. For both directions of rotation the probability distribution showed two peaks. The respective forward directed peak was narrower and taller than the one where the enzyme had snapped back after being pressed to its forward limiting position. When the magnetic field was off, the bead fluctuated approximately around the middle position of its forced rotation. If, in some single molecules, this approximate symmetry was absent (dominating surface contacts?) the respective data were discarded. The reproducibility of the thermal fluctuations after switching off the magnetic field after a counter-clockwise and a clockwise turn is demonstrated by the red and the blue histograms in the upper part of Fig. 4B. From the FWHM of these distributions, about  $7^\circ$ , the torsional stiffness of the eccentric bearing was calculated, 1500 pNnm.

## SUMMARY AND DISCUSSION

Fig. 5 summarizes the data. It shows a section through the enzyme in gray, and in color the cysteine pairs serving to establish a disulfide lock between rotor and stator. The total stiffness,  $\kappa_{\text{total}}$ , as detected when closing the respective disulfide bridge, is indicated in matching color at the horizontal bar. The partial stiffness of certain subsections of the enzyme are indicated at the vertical arrows. The bottom line is as follows: (i) The thin end of the rotor, i.e. the coiled coil portion plus the C-terminal helix of subunit  $\gamma$  is of medium stiffness ( $\kappa \cong 750 \text{ pNnm}$ ), (ii) both the bulk of  $F_1$ ,  $(\alpha\beta)_3$ , and the eccentric stator are very stiff ( $\kappa \cong 1500 \text{ pNnm}$ ), (iii) only the enzyme portion between  $\gamma 87C$ , subunit  $\epsilon$  and the **c**-ring is more compliant ( $\kappa \cong 68 \text{ pNnm}$ ), (iv) the most compliant domain is located between the sites where the respective power strokes in  $F_1$  and  $F_O$  are generated (red arrow), i.e. where good mechanical engineering would have placed it, and (v) if the DELSEED lever is free to undergo hinge motion, as during the ATP-waiting dwell, it contributes another rotary torsional compliance with a stiffness of about 50 pNnm.

Hydrolysis of ATP by EF<sub>O</sub>F<sub>1</sub> produces an average torque of 50 pNnm as determined from the curvature of a F<sub>O</sub>-attached actin-filament by the same single molecule set-up illustrated in Fig. 2A (4). If the holoenzyme operates in its native coupling membrane, and if it reaches thermodynamic equilibrium then the forward torque generated by ionmotive force (by F<sub>O</sub>) counterbalances the backward torque by ATP hydrolysis (by F<sub>1</sub>), and the elastic element between them is maximally wound up. Taking the above determined stiffness of the most compliant domain of EF<sub>O</sub>F<sub>1</sub> as 68 pNnm, it implies that the rotor is twisted by an angle of  $\phi = \frac{M}{\kappa} = \frac{50}{68} = 0.74 \text{ radian}$  or 42°, whereas the eccentric bearing is only negligibly twisted by

<2°. This amounts to the storage of elastic energy of  $U = \frac{M^2}{2\kappa} = 18 \text{ pNnm}$  or 11.1 kJ/mol.

How do these figures compare with those that have been hypothesized or indirectly inferred in previous studies?

Simulations of the kinetic behaviour of the enzyme taking the transient storage of elastic energy have led to gross estimates for the torsional stiffness of the elastic buffer, 60 pNnm (13) and 30 pNnm (14), respectively. A stored elastic energy (6 k<sub>B</sub>T → 24.7 pNnm → 14.9 kJ/mol) has been calculated for the elastic hinge motion in subunit β (15). The former figures resulted from rather indirect kinetic or theoretical approaches. The experimentally observed smoothing of the discrete power strokes of F<sub>1</sub> after being transmitted to F<sub>O</sub> has led to an estimate for stiffness in the order of 60 pNnm (4). The figures for the stiffness of the major elastic element between F<sub>O</sub> and F<sub>1</sub> resulting from the present work,  $\kappa \cong 68 \text{ pNnm}$ , and for the buffered elastic energy,  $U \cong 11 \text{ kJ/mol}$ , are of the same magnitude as the former ones. For the first time, however, the elastic buffer was experimentally attributed to a given domain, namely the bulky segment including the large, globular domains of subunits γ and ε plus the loops of the ring of subunit c to which they are attached.

Our results qualified the role of three enzyme domains that were tentatively discussed in this role: (i) The eccentric bearing was rather stiff (see Fig. 4B) (for the large binding strength of subunits  $\delta$  and  $\mathbf{b}_2$  to the hexagon of  $(\alpha\beta)_3$  see (22-24) and for a comprehensive review on  $\mathbf{b}_2$  see (21)). (ii) The elasticity of the hinge motion of the DELSEED region of subunit  $\beta$  has been previously emphasized in a theoretical studies (15, 25). We have found that it matters during the turnover of the active enzyme, but it is not the main determinant of the elastic power transmission. (iii) When discussing the inner elasticity of  $F_0F_1$  several groups (e.g. (26)) including our own have emphasized a role of the coiled coil plus the extended C-terminal end of subunit  $\gamma$ . Deletion studies (27, 28) have shown that this portion of the enzyme, extending from the counterpart on subunit  $\gamma$  of the DELSEED-domain towards the supposed "hydrophobic bearing" (6), is dispensable for torque generation by  $F_1$ , although being helpful for enzyme assembly and stability (27). Being (a) much less compliant than the main elastic buffer associated with the globular portions of  $\gamma$  and  $\epsilon$ , and (b) mobile in its bearing (29, 30) the coiled coil region of subunit  $\gamma$  cannot be claimed as the main elastic buffer.

That the main compliance is associated with the globular portions of  $\gamma$  and  $\epsilon$  in contact with the c-ring is in line with the observation that these enzyme domains are not well resolved in crystals of both  $F_1$  (6) and  $F_0F_1$  (11). Our data provide a basis for testing the predictive power of normal mode analysis (31) and molecular dynamics simulations (31-36) of this particularly agile enzyme.

Because of the existence of an elastic buffer between the two stepping rotary motors in ATP synthase any fine tuning between the partial ion transport events occurring in  $F_0$  and the partial chemical reactions (e.g. cleavage of certain hydrogen bonds) in  $F_1$  is dispensable. The elastic power transmission explains why the enzyme can work by the same principles with different gears (3:10-15) in different organisms, and why it operates robustly even in structurally modified

(27, 28, 37-39) and in chimeric constructs with F<sub>O</sub> and F<sub>1</sub> taken from different sources (40). The essential function of the elastic buffer is to provide this stepping rotary enzyme with high kinetic efficiency, in other words with a high rate of turnover under load (3, 4).

## Materials and Methods

### Molecular Genetics

This work was carried out with three plasmids, namely pKH4, pSE1, and pKH7, and their derivatives. pKH4, the starting plasmid, had all wild-type cysteines substituted by alanines, and carried a His<sub>6</sub>-tag at the N-terminal of subunit  $\beta$  (41). The plasmid pSE1, based on pKH4, carried a Strep-tagged C-terminal in subunit  $c$  (16). The plasmid pKH7, based on pKH4, carried one extra cysteine,  $\gamma$ K108C. The plasmid pSW3, based on pKH7, carried the cysteine pair  $\beta$ D380C/ $\gamma$ A87C and is described in (42). The pKH7 based plasmid pMM25, carrying the cysteine pair  $\alpha$ E284C/ $\gamma$ A270C, was a kind gift of M. Müller.

pSE1 was used as the starting plasmid for the mutations  $\alpha$ E284C/ $\gamma$ L276C, **a**l223C/**c**L72C, and  $\beta$ D380C/ $\gamma$ A87C, resulting in the plasmids pGH14, pGH33, and pGH47, respectively. pBluescript II SK (+/-) subclones were generated by insertion of the following fragments of pSE1: *KpnI/XhoI* and *KpnI/SacI* for pGH14, *BamHI/HindIII* and *BsrGI/PpuM*. for pGH33, and *KpnI/SacI* for  $\gamma$ A87C in pGH47. Site-directed mutagenesis was carried out by polymerase chain reaction using the oligonucleotide 5'-CGCCAGGACGTTTGTGCATTC<sup>CGG</sup>-3' and its complement 5'-CCGGGAATGCACAACGTCCTGGCG-3' for  $\alpha$ E284C, 5'-GCATTACTCAGG AATGCACCGAGATCGTCTCG-3' and its complement 5'-CGAGACGATCTCGGTGCATTCC TGAGTAATGC-3' for  $\gamma$ L276C, 5'-CCGGTGAGCTGATTTTCTTGTCTGATTGCTGGTCTGTT GC-3' and its complement 5'-GCAACAGACCAGCAATCAGACAGAAAATCAGCTCACCG G-3' for **a**l223C, 5'-CGCTGTAGGTCTGGGTTGCTACGTGATGTTTCGCTGTC-3' and its complement 5'-GACAGCGAACATCACGTAGCAACCCAGACCTACAGCG-3' for **c**L72C, and 5'-CGACCGACCGTGGTTTGTTGTGGTGGTTTGAAC-3' and its complement 5'-GTTCA

AACCACCACACAAACCACGGTCGGTCG-3 for  $\gamma$ A87C (43). *KpnI/XhoI*, *BsrGI/PpuM*, and *KpnI/SacI* fragments of pSE1 were substituted with the corresponding fragments carrying the  $\alpha$ E284C, cL72C, and  $\gamma$ A87C mutations by standard restriction and ligation resulting in plasmids pKG7, pGH39, and pGH46, respectively. The double mutants  $\alpha$ E284C/ $\gamma$ L276C, and aI223C/cL72C were then generated by exchanging the *KpnI/SacI* and *BamHI/HindIII* fragments of pKG7 and pGH39 with the corresponding mutated fragments of the pBluescript II SK (+/-) subclones by standard restriction and ligation, resulting in the plasmids pGH14, and pGH33, respectively. The plasmid pGH47 was obtained by exchanging *XbaI/SacI* fragment of pGH46 with the respective fragment of pSW3, carrying the mutation  $\beta$ D380C, by standard restriction and ligation. Successful cloning was checked by nucleotide sequencing.

A cysteine residue was added to the N-terminus of the **b** subunit by site-directed mutagenesis by the following procedures. A 756-bp *BsaHI* fragment of pKH4 including the gene for subunit **c** and most of the gene for subunit **b** was cloned into pUC8 that had been cut with *AccI* to produce pSD300, with the insert in the reverse orientation relative to expression. Site-directed mutagenesis was carried out by polymerase chain reaction using pSD300 as the template with the mutagenic oligonucleotide 5'-CAGAACGTTAACTAAATAGAGGCATTGTGCT GTGAATTGTATGAATCTTAACGCAACAATC-3' and the M13 reverse primer. The mutagenic oligonucleotide included the *HpaI* site (*italics*) located upstream of the uncF start codon, and a three codon insertion (underlined) at the start of uncF, retaining the natural GUG start codon. This insertion changed the N-terminal amino acid sequence encoded from MNLN to MNCMNLN. The PCR product was cut with *HpaI* and *EcoRI*, and inserted into pSD300 that had been cut with the same enzymes to produce plasmid pSD303. After DNA sequencing, this plasmid was cut with *PpuMI* and *BsrGI* and the 431-bp fragment was inserted into pKH4 that had been cut at unique sites with the same enzymes to produce plasmid pSD308.

#### **Preparation of EF<sub>1</sub> and EF<sub>0</sub>F<sub>1</sub>**

The preparation of EF<sub>1</sub>, derived from the plasmids pSW3 and pMM25, followed the same procedures published previously (27, 42).

EF<sub>0</sub>F<sub>1</sub>, derived from the plasmids pGH14, pGH33, and pGH47, was prepared and purified via its Strep-tags as described in elsewhere (16).

EF<sub>0</sub>F<sub>1</sub> based on pSD308, lacking the Strep-tag in **c**, was purified via its His-tags as follows: Membrane protein was obtained as above followed by centrifugation at 100000 x g for 90 min. The supernatant was diluted with buffer A (20 mM Tris/HCl (pH 7,5); 50 mM KCl; 5 mM MgCl<sub>2</sub>; 10 % (v/v) glycerol; 20 mM imidazole) to 1 % (w/v) N-octyl-L-D-glucopyranoside final concentration and applied (thrice) to an empty NAP5 column packed with 1 ml of Ni-NTA-Superflow. Wash was done with 5 ml buffer A and then with the same buffer containing 150 mM imidazole.

70% glycerol were added to eluates before they were quick-freezed in liquid nitrogen and stored at -80 °C prior to use.

### **Preparation of F-actin**

The preparation of F-actin followed the same procedures published previously (16).

### **Preparation of magnetic beads**

Streptavidin coated hyper-paramagnetic beads (Roche, Mannheim, Germany; stock solution 10 mg/ml, diameter 1 µm) for experiments with EF<sub>1</sub> or EFOF<sub>1</sub> were diluted tenfold with 50 mM MOPS/KOH (pH 7.5), 50 mM KCl, and 5 mM MgCl<sub>2</sub> (buffer B) or 50 mM MOPS/KOH (pH 7.5), 50 mM KCl, 5 mM MgCl<sub>2</sub>, 0.5% (w/v) N-octyl-L-D-glucopyranoside, and 10% (v/v) glycerol (buffer C), respectively. The dilute suspension was centrifuged (16.000 x g, 4 °C, 3 min) and the pellet was resuspended in buffer B or C. This washing procedure was repeated three times.

### **Immobilization of EF<sub>1</sub> and EF<sub>0</sub>F<sub>1</sub>**

Similar procedures were used for immobilizing EF<sub>1</sub> and EF<sub>0</sub>F<sub>1</sub>. Samples were filled into flow cells consisting of two cover-slips (bottom 26x76 mm<sup>2</sup>; top 24x24 mm<sup>2</sup>) separated by double adhesive tape (Tesa, Hamburg, Germany). EF<sub>0</sub>F<sub>1</sub> protein solutions were stepwise infused as previously (16), using buffer C in all steps. 50 μM - 5 mM ATP were used in the last step. For ADP inhibition 50 μl of 20 mM glucose, 0.2 mg/ml glucose oxidase, 50 μg/ml catalase (oxygen scavenger system, OSS), 0.5% 2-mercaptoethanol (2-me), 1 U/μl hexokinase, and 5 mM ADP in buffer C were added after washing with 50 μl of buffer C.

The infusion order for EF<sub>1</sub> was as follows (50 μl per step, 4 min incubation, wash with buffer B before each step): (1) 0.8 μM Ni-NTA-horseradish peroxidase conjugate in buffer B; (2) 10 mg/ml bovine serum albumine in buffer B; (3) 5 μM EF<sub>1</sub> in buffer B; (4) 0.2 mg/ml magnetic beads in buffer B (7 min incubation); (5) 2 pM Q-dots (Quantum Dot Corporation, Hayward, CA, USA; stock 2 μM, dilution factor 1:1.000.000) in buffer B (7 min incubation); (6) OSS, 0.5% 2-me, 20 mM DTT, and 5 mM ATP in buffer B. For pSD308-based EF<sub>0</sub>F<sub>1</sub> the infusion followed the same instructions as for EF<sub>1</sub> (without 20mM DTT in step 6), but replacing buffer B to buffer C.

For oxidization of both, EF<sub>0</sub>F<sub>1</sub> and EF<sub>1</sub>, 50 μl of OSS, 0.2 mg/ml creatine kinase, 2.5 mM creatine phosphate, 1-2 mM Ellman's reagent, and 5 mM ATP in buffer C or B were added after washing with 50 μl of buffer C or B, respectively. For reducing of EF<sub>1</sub> after oxidization 50 μl of OSS, 0.5% 2-me, 20 mM DTT, 10 mM Na<sub>2</sub>S<sub>2</sub>O<sub>4</sub>, and 5 mM ATP in buffer B were added after washing with 50 μl of buffer B.

### **Video-microscopy**

EF<sub>1</sub> and EF<sub>0</sub>F<sub>1</sub> constructs were observed and single molecule rotation was recorded with an inverted fluorescence microscope as published previously (16). Fast bleaching of the fluorescently labeled actin filaments in the oxidized state was overcome by reducing the excitation intensity. Video data were captured with a Pinnacle DV500 Plus video card, and



digitised with Adobe Premiere 6.0. A software for evaluation of the obtained video sequences was written with Matlab 7.

### **Homology modelling**

Our model of  $EF_0F_1$  was based upon the structure as determined by Abrahams *et al.* (1bmf, (6)). Modeling was carried out with the programs WhatIf (44) and O (45). The model coordinates are available from <http://www.biologie.uni-osnabrueck.de/Biophysik/Engelbrecht/se/data/ef1/>.

### **Acknowledgements**

The authors are very grateful for excellent technical assistance by Gaby Hikade and Yumin Bi (molecular biology), and Hella Kenneweg (single molecule microscopy). They acknowledge financial support by the Deutsche Forschungsgemeinschaft (SFB431/P1 to SE), the European Union (to WJ and SE), the Volkswagen Foundation (to WJ), the Fonds der Chemie (to WJ), and Canadian Institutes of Health Research (to SD).

### **References**

1. Junge, W, Lill, H, Engelbrecht, S (1997) ATP synthase: an electrochemical transducer with rotatory mechanics. *Trends Biochem Sci* 22: 420-423.
2. Wang, HY, Oster, G (1998) Energy transduction in the  $F_1$  motor of ATP synthase. *Nature* 396: 279-282.
3. Junge, W et al. (2001) Inter-subunit rotation and elastic power transmission in  $F_0F_1$ -ATPase. *FEBS Lett* 504: 152-160.
4. Pänke, O, Cherepanov, DA, Gumbiowski, K, Engelbrecht, S, Junge, W (2001) Viscoelastic dynamics of actin filaments coupled to rotary F-ATPase: Torque profile of the enzyme. *Biophys J* 81: 1220-1233.
5. Jiang, W, Hermolin, J, Fillingame, RH (2001) The preferred stoichiometry of c subunits in the rotary motor sector of Escherichia coli ATP synthase is 10. *Proc Natl Acad Sci* 98: 4966-4971.
6. Abrahams, JP, Leslie, AGW, Lutter, R, Walker, JE (1994) The structure of  $F_1$ -ATPase from bovine heart mitochondria determined at 2.8 Å resolution. *Nature* 370: 621-628.
7. Nishizaka, T et al. (2004) Chemomechanical coupling in  $F_1$ -ATPase revealed by simultaneous observation of nucleotide kinetics and rotation. *Nat Struct Mol Biol* 11: 142-148.
8. Shimabukuro, K et al. (2003) Catalysis and rotation of  $F_1$  motor: cleavage of ATP at the catalytic site occurs in 1 ms before 40 degree substep rotation. *Proc Natl Acad Sci* 100: 14731-14736.

9. Yasuda, R, Noji, H, Yoshida, M, Kinoshita, K, Jr., Itoh, H (2001) Resolution of distinct rotational substeps by submillisecond kinetic analysis of F<sub>1</sub>-ATPase. *Nature* 410: 898-904.
10. Pogoryelov, D et al. (2007) The C<sub>15</sub>-ring of the *Spirulina platensis* F-ATP synthase: F<sub>1</sub>/F<sub>0</sub> symmetry mismatch is not obligatory. *EMBO Rep* 6: 1040-1044.
11. Stock, D, Leslie, AG, Walker, JE (1999) Molecular architecture of the rotary motor in ATP synthase. *Science* 286: 1700-1705.
12. Junge, W, Nelson, N (2005) Nature's Rotary Electromotors. *Science* 308: 642-644.
13. Cherepanov, DA, Mulikidjanian, A, Junge, W (1999) Transient accumulation of elastic energy in proton translocating ATP synthase. *FEBS Lett* 449: 1-6.
14. Pänke, O, Rumberg, B (1999) Kinetic modeling of rotary CF<sub>0</sub>F<sub>1</sub>-ATP synthase: storage of elastic energy during energy transduction. *Biochim Biophys Acta* 1412: 118-128.
15. Sun, S, Chandler, D, Dinner, AR, Oster, G (2003) Elastic energy storage in beta-sheets with application to F<sub>1</sub>-ATPase. *Eur Biophys J* 32: 676-683.
16. Pänke, O, Gumbiowski, K, Junge, W, Engelbrecht, S (2000) F-ATPase: specific observation of the rotating c subunit oligomer of EF<sub>0</sub>EF<sub>1</sub>. *FEBS Lett* 472: 34-38.
17. Cherepanov, DA, Junge, W (2001) Viscoelastic dynamics of actin filaments coupled to rotary F-ATPase: Curvature as an indicator of the torque. *Biophys J* 81: 1234-1244.
18. Tsunoda, SP et al. (2000) Observations of rotation within the F<sub>0</sub>F<sub>1</sub>-ATP synthase: deciding between rotation of the F<sub>0</sub>c subunit ring and artifact. *FEBS Lett* 470: 244-248.
19. Del Rizzo, PA, Bi, Y, Dunn, SD, Shilton, BH (2002) The "second stalk" of Escherichia coli ATP synthase: structure of the isolated dimerization domain. *Biochemistry* 41: 6875-6884.
20. Revington, M, Dunn, SD, Shaw, GS (2002) Folding and stability of the b subunit of the F(1)F(0) ATP synthase. *Protein Sci* 11: 1227-1238.
21. Dunn, SD, Revington, M, Cipriano, DJ, Shilton, BH (2000) The b subunit of Escherichia coli ATP synthase. *J Bioenerg Biomembr* 32: 347-355.
22. Häsler, K, Pänke, O, Junge, W (1999) On the stator of rotary ATP synthase: the binding strength of subunit delta to (αβ)<sub>3</sub> as determined by fluorescence correlation spectroscopy. *Biochemistry* 38: 13759-13765.
23. Weber, J, Wilke-Mounts, S, Nadanaciva, S, Senior, AE (2004) Quantitative determination of direct binding of b subunit to F<sub>1</sub> in Escherichia coli F<sub>1</sub>F<sub>0</sub>-ATP synthase. *J Biol Chem* 279: 11253-11258.
24. Diez, M et al. (2004) Binding of the b-subunit in the ATP synthase from Escherichia coli. *Biochemistry* 43: 1054-1064.
25. Ma, J et al. (2002) A dynamic analysis of the rotation mechanism for conformational change in F(1)-ATPase. *Structure* 10: 921-931.
26. Menz, RI, Walker, JE, Leslie, AG (2001) Structure of bovine mitochondrial F(1)-ATPase with nucleotide bound to all three catalytic sites: implications for the mechanism of rotary catalysis. *Cell* 106: 331-341.
27. Müller, M, Pänke, O, Junge, W, Engelbrecht, S (2002) F<sub>1</sub>-ATPase: The C-terminal end of subunit γ is not required for ATP hydrolysis-driven rotation. *J Biol Chem* 277: 23308-23313.
28. Hossain, MD et al. (2006) The rotor tip inside a bearing of a thermophilic F<sub>1</sub>-ATPase is dispensable for torque generation. *Biophys J* 90: 4195-4203.
29. Muller, M et al. (2004) Rotary F<sub>1</sub>-ATPase. Is the C-terminus of subunit gamma fixed or mobile? *Eur J Biochem* 271: 3914-3922.

30. Sabbert, D, Engelbrecht, S, Junge, W (1996) Intersubunit rotation in active F-ATPase. *Nature* 381: 623-625.
31. Cui, Q, Li, G, Ma, J, Karplus, M (2004) A normal mode analysis of structural plasticity in the biomolecular motor F(1)-ATPase. *J Mol Biol* 340: 345-372.
32. Bockmann, RA, Grubmuller, H (2002) Nanoseconds molecular dynamics simulation of primary mechanical energy transfer steps in F1-ATP synthase. *Nat Struct Biol* 9: 198-202.
33. Yang, W, Gao, YQ, Cui, Q, Ma, J, Karplus, M (2003) The missing link between thermodynamics and structure in F1-ATPase. *Proc Natl Acad Sci* 100: 874-879.
34. Dittrich, M, Hayashi, S, Schulten, K (2003) On the mechanism of ATP hydrolysis in F1-ATPase. *Biophys J* 85: 2253-2266.
35. Bockmann, RA, Grubmuller, H (2003) Conformational dynamics of the F1-ATPase beta-subunit: a molecular dynamics study. *Biophys J* 85: 1482-1491.
36. Pu, J, Karplus, M (2008) How subunit coupling produces the gamma-subunit rotary motion in F1-ATPase. *Proc Natl Acad Sci* 105: 1192-1197.
37. Cipriano, DJ, Bi, Y, Dunn, SD (2002) Genetic fusions of globular proteins to the epsilon subunit of the Escherichia coli ATP synthase: Implications for in vivo rotational catalysis and epsilon subunit function. *J Biol Chem* 277: 16782-16790.
38. Sorgen, PL, Caviston, TL, Perry, RC, Cain, BD (1998) Deletions in the second stalk of F<sub>1</sub>F<sub>0</sub>-ATP synthase in Escherichia coli. *J Biol Chem* 273: 27873-27878.
39. Sorgen, PL, Bubb, MR, Cain, BD (1999) Lengthening the second stalk of F(1)F(0) ATP synthase in Escherichia coli. *J Biol Chem* 274: 36261-36266.
40. Kaim, G, Dimroth, P (1995) Formation of a functionally active sodium-translocating hybrid F<sub>1</sub>F<sub>0</sub> ATPase in *Propionigenium modestum* by homologous recombination. *Eur J Biochem* 218: 937-944.
41. Noji, H et al. (1999) Rotation of Escherichia coli F(1)-ATPase. *Biochem Biophys Res Comm* 260: 597-599.
42. Gumbiowski, K et al. (2001) F-ATPase: forced full rotation of the rotor despite covalent cross-link with the stator. *J Biol Chem* 276: 42287-42292.
43. Weiner, MP et al. (1994) Site-directed mutagenesis of double-stranded DNA by the polymerase chain reaction. *Gene* 151: 119-123.
44. Vriend, G (1990) WHAT IF: a molecular modeling and drug design program. *J Mol Graph* 8: 52-6, 29.
45. Jones, TA, Zou, JY, Cowan, SW, Kjeldgaard (1991) Improved methods for binding protein models in electron density maps and the location of errors in these models. *Acta Crystallogr A* 47: 110-119.
46. Sielaff, H, Rennekamp, H, Engelbrecht, S, Junge, W (2008) Functional halt positions of rotary F<sub>0</sub>F<sub>1</sub>-ATPase correlated with crystal structures. *Biophysical J*. 95 -in press-

## Figure Legends

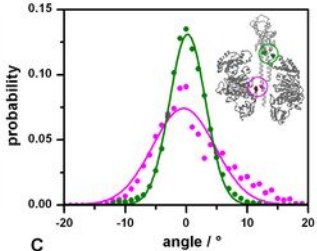
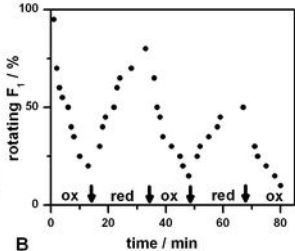
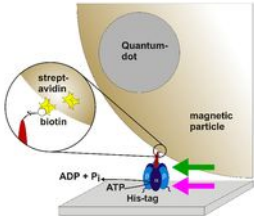
**Fig. 1** Immobilized  $EF_1$  with attached magnetic bead (A), the yield of magnetically forced rotation as function of oxidation-reduction cycles (B), and histograms of thermally driven rotational fluctuations (magnetic field off) after the formation of a disulfide cross link between the rotor and the stator (C). The green and magenta arrows in Fig. 1A indicates the position of the particular disulfide cross links in the homology model of  $EF_1$  (inset in C) that are encircled in green and magenta in C, respectively. The arrows in B indicate the time, when the solution was changed from reducing to oxidizing and *vice versa*. The points in C are experimental and the lines are the respective fits by a single Gaussian. For details, see text.

**Fig. 2** Immobilized  $EF_0F_1$  with attached actin filament of short length, typ.  $0.5\ \mu\text{m}$  (A), and histograms of thermally driven rotational fluctuations after the formation of a disulfide cross link between the rotor and the stator (B). The positions of three different disulfide cross links are indicated in colors in A and in the inset in B, with matching colors of the respective histograms. For details, see text.

**Fig. 3** Rotary trajectory under hydrolysis of ATP by active  $EF_0F_1$  (A) and histogram of a more extended trajectory (B). The trajectory was recorded at  $50\ \mu\text{M}$  ATP with  $5\ \text{mM}$   $\text{Mg}^{2+}$  present. As discussed elsewhere (46), the halt positions represent the ATP-waiting dwells which follow each other with a period of  $120^\circ$ . The duration of these dwells, some  $100\ \text{ms}$ , was typical for immobilized  $EF_0F_1$ . The waiting for ATP-binding was *not* diffusion controlled. The orange histogram represents fluctuations after the molecule has fallen into its ADP-saturated state. Its peak was always displaced by  $-40^\circ$  relative to the nearest one of the three ATP-waiting dwells. Details of the relation between the stepping motion and the crystal structure have been published elsewhere (46).

**Fig. 4** Immobilized  $EF_0F_1$  with a Q-dot doped magnetic bead attached to the C-terminal end of both copies of subunit **b** (A) and histograms of rotary fluctuations (B) with the magnetic field off (top) and slowly (0.125 rev/s) rotating (bottom). The rotation was either clockwise (when viewed from the  $F_0$ -side), shown in blue, or counter-clockwise, in red. The fluctuations in the absence of the magnetic field (top) shown in blue and red, respectively, were observed subsequent of a previous clockwise and counter-clockwise motion. The points are experimental and the lines fits with a single Gaussian (top) and with two Gaussians each (bottom).

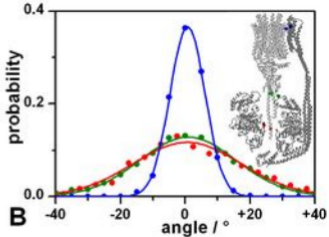
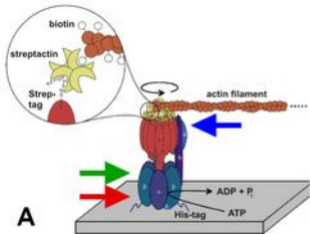
**Fig. 5** Structural model of  $EF_0F_1$  (stator subunits in dark gray, rotor in light gray), and, at the very right side, of the homodimer of subunit **b**, and numbers for the torsional stiffness of various domains. Numbers given on the left side resulted from data obtained with  $EF_1$  in the set-up shown in Fig. 1A, those in the right side from  $EF_0F_1$  as in Fig. 2A, and the one at the very right from  $EF_0F_1$  as in Fig. 4A. The stiffness  $\kappa$  comes in units of pNm. Numbers associated with horizontal colored lines denote the resulting stiffness  $\kappa_{result}$  (see Eq. 3) as observed when the respective disulfide cross link (its two cysteines shown in the same hue, dark on the stator or light on the rotor) was closed. The numbers between the black vertical arrows denote the stiffnesses of the rotor domain lying between the respective pairs of cross link positions. The red arrow marks the region of greatest compliance in  $EF_0F_1$ , the dominant elastic buffer which is responsible for an elastic power transmission between  $F_0$  and  $F_1$ .

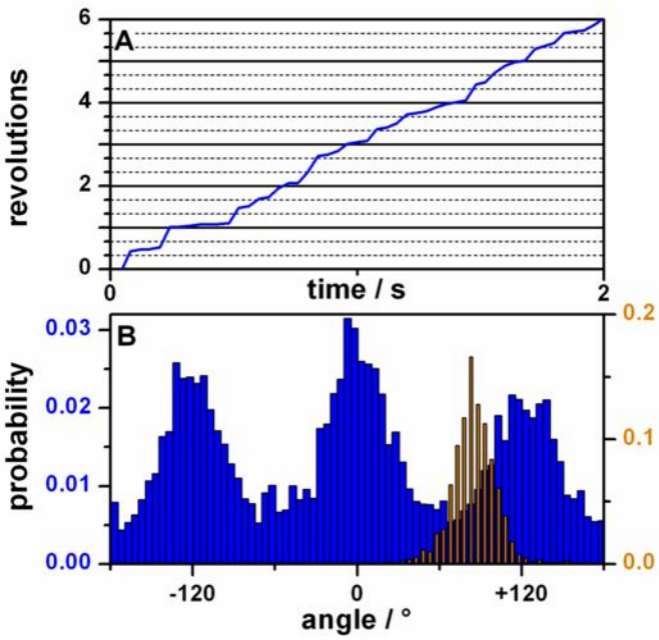


A

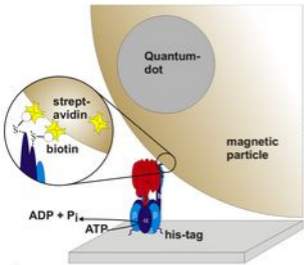
B

C

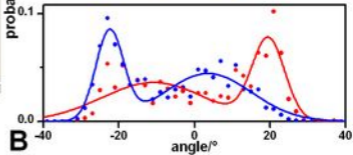
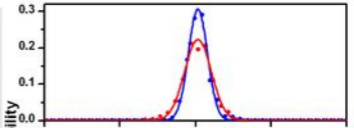








**A**



**B**

rotor

stator

$EF_1$

$EF_0F_1$

$EF_0F_1$

—1500

